IEICE TRANS. INF. & SYST., VOL.E93–D, NO.9 SEPTEMBER 2010

PAPER

Signal and Noise Covariance Estimation Based on ICA for High-Resolution Cortical Dipole Imaging

Junichi HORI[†a)], ***Member***, **Kentarou SUNAGA**[†*], ***and*** **Satoru WATANABE**[††**], ***Nonmembers***

SUMMARY We investigated suitable spatial inverse filters for cortical dipole imaging from the scalp electroencephalogram (EEG). The effects of incorporating statistical information of signal and noise into inverse procedures were examined by computer simulations and experimental studies. The parametric projection filter (PPF) and parametric Wiener filter (PWF) were applied to an inhomogeneous three-sphere volume conductor head model. The noise covariance matrix was estimated by applying independent component analysis (ICA) to scalp potentials. The present simulation results suggest that the PPF and the PWF provided excellent performance when the noise covariance was estimated from the differential noise between EEG and the separated signal using ICA and the signal covariance was estimated from the separated signal. Moreover, the spatial resolution of the cortical dipole imaging was improved while the influence of noise was suppressed by including the differential noise at the instant of the imaging and by adjusting the duration of noise sample according to the signal to noise ratio. We applied the proposed imaging technique to human experimental data of visual evoked potential and obtained reasonable results that coincide to physiological knowledge.

key words: *EEG, cortical dipole imaging, spatial inverse filter, covariance, independent component analysis*

1. Introduction

Electroencephalogram (EEG) has been a useful modality to provide high temporal resolution of underlying brain electrical activity. However, the spatial resolution of EEG is limited due to the smearing effect of the head volume conductor [1], [2]. It is therefore important to develop high resolution imaging techniques to enhance the spatial resolution of EEG. Among the approaches which attempt to correct the smearing effect, of interest is the spatial enhancement approaches, which attempt to deconvolve the low-pass spatial filtering effect of volume conduction of the head [3]–[12]. For review, see reference [13]. Equivalent dipole imaging has been proposed to estimate the high-resolution cortical dipole layer distribution to account for the scalp potential [3], [4], [14]. In this model, the electrical sources inside of the brain are equivalently represented by the dipole distribution on the dipole layer. The cortical dipole imaging provides the advantage that high-resolution brain electrical activity can be estimated without an ad hoc assumption about the number and the orientation of source dipoles. The cortical dipole imaging requires solving an inverse problem described by the transfer function from the scalp potentials to the dipole layer. We have developed an inverse procedure for cortical dipole source imaging using a parametric projection filter (PPF) which enables estimation of inverse solutions in the presence of noise information [15]–[17]. Information related to noise distribution, as defined by the covariance matrix, was assumed to be known. Our previous results indicated that the PPF provided a better approximation to the original dipole distribution than that of traditional inverse techniques in the case of low correlation between signal and noise distributions. Moreover, Wiener reconstruction frameworks based on both signal and noise covariance matrices have been also investigated [18]–[20]. We applied the parametric Wiener filter (PWF) to the inverse problem of the cortical dipole imaging [21].

In order to realize high-resolution brain functional imaging using the PPF or the PWF, it is necessary to estimate the signal and noise components in accuracy. In clinical and experimental setting, the noise covariance might be estimated from data that are known to be source-free, such as pre-stimulus data in evoked potentials [22], [23]. Then, the signal covariance was calculated from the estimated noise covariance. However, it was difficult to distinguish the noise from EEG data. In this study, the noise covariance matrix was estimated from the noise components which were separated by applying independent component analysis (ICA) [24] to the observed EEG signals. ICA extracts independent sources from the observed signal based on statistical independence of the original signal. It has been applied to extract the features of the individual signal components or reject the noise or artifact components [25]. In the present study, we supposed that the signal and noise are independent of each other. For estimating the noise covariance, we investigated how to extract the noise component from EEG signals. The noise covariance matrix was calculated from the separated noise using ICA or the difference noise between the scalp EEG signal and the separated signal. The signal covariance in the PWF was calculated with either the measured EEG or the separated signal using ICA. Moreover, the suitable sampling method of noise information was examined for improving the performance of the spatial inverse filter by computer simulations and human experimental studies.

Manuscript received January 15, 2010.
Manuscript revised May 24, 2010.

[†]The authors are with the Graduate School of Science and Technology, Niigata University, Niigata-shi, 950–2181 Japan.
[††]The author is with the Department of Biocybernetics, Niigata University, Niigata-shi, 950–2181 Japan.
[*]Presently, with Hitachi Medical Corp.
[**]Presently, with Olympus Medical Systems Corp.
a) E-mail: hori@eng.niigata-u.ac.jp

DOI: 10.1587/transinf.E93.D.2626

2. Method

2.1 Cortical Dipole Imaging

In the cortical dipole imaging study, the head volume conductor was approximated by an inhomogeneous three-concentric sphere model [26]. Dipoles are uniformly distributed over a sphere inside of the brain. This model incorporates variation in conductivity of different tissues such as the scalp, the skull, and the brain. It has been used to provide a reasonable approximation to head volume conductor for the cortical dipole imaging. An equivalent dipole layer within the brain simulates the brain electrical activity. The transfer matrix from the dipole layer to the scalp potential is obtained by considering the geometry of the model and the physical relationships among the quantities involved. The dipole layer distribution is reconstructed from the recorded scalp potential by solving an inverse problem of the transfer matrix.

The observation system of brain electrical activity on the scalp surface is defined using the following equation:

$$\mathbf{g} = \mathbf{A}\mathbf{f} + \mathbf{n} \tag{1}$$

where $\mathbf{f}$ is the vector of the equivalent dipole sources distributed over the dipole layer, $\mathbf{n}$ is the additive noise, and $\mathbf{g}$ is the scalp potential. In addition, $\mathbf{A}$ represents the transfer matrix from the equivalent dipole sources to the scalp potential signals. It is important to infer the origins from the recorded EEG and to map the sources that generate the scalp EEG. Thus, the inverse problem is defined as

$$\mathbf{f}_0 = \mathbf{B}\mathbf{g} \tag{2}$$

where $\mathbf{B}$ is the inverse filter from the scalp EEG to the dipole layer distribution and $\mathbf{f}_0$ is the estimated source distribution of the dipole layer. Because the number of measurement electrodes is always much smaller than the dimensions of the unknown vector $\mathbf{f}$, this problem is an underdetermined inverse problem.

2.2 Spatial Inverse Filter

Several inverse techniques have been proposed to solve such inverse problems. In the presence of noise, the truncated singular value decomposition [27] or Tikhonov regularization method [28] can be used to calculate the pseudo inverse filter. The PPF, which allows estimating solutions in presence of information on noise covariance structure, has been introduced to solve the inverse problem [29]. The PPF is given by

$$\mathbf{B} = \mathbf{A}^T(\mathbf{A}\mathbf{A}^T + \gamma\mathbf{Q})^{-1} \tag{3}$$

where γ is a positive number known as the regularization parameter and $\mathbf{A}^T$ the transpose matrix of $\mathbf{A}$. The matrix $\mathbf{Q}$ is the noise covariance derived from the expectation over the noise ensemble $\mathrm{E}[\mathbf{n}\mathbf{n}^T]$. The regularization parameter γ controls the mutual weights of two terms. The determination of the value of parameter γ is left to the subjective judgment of the user. We have developed a criterion that estimates the optimum parameter using iterative calculation for restoration [15]. The criterion estimates the parameter that minimizes the approximated error between the original and estimated source signals without knowing the original source distribution.

When statistical information of the signal and noise are presented, the parametric Wiener filter can be applied to the inverse problem [18]–[21]. Suppose $\mathbf{R}$ the signal covariance, which can be derived from the expectation over the signal $\mathbf{f}$ ensemble, $\mathrm{E}[\mathbf{f}\mathbf{f}^T]$. The PWF is derived by

$$\mathbf{B} = \mathbf{R}\mathbf{A}^T(\mathbf{A}\mathbf{R}\mathbf{A}^T + \gamma\mathbf{Q})^{-1} \tag{4}$$

If $\mathbf{R} = \mathbf{Q} = \mathbf{I}$ (the identity matrix), then Eq. (4) is reduced to the zero-order Tikhonov regularization method. If $\mathbf{R} = \mathbf{I}$, then Eq. (4) is reduced to the PPF that considers just the covariance matrix of the noise distribution $\mathbf{Q}$ as shown in Eq. (3).

We have to estimate the signal and noise covariance matrices to construct the PPF or the PWF. If we can obtain the time-varying noise component $n_i(t)$ on the electrode number i, each element of the matrix $\mathbf{Q}$ at the time instant t' is approximated from

$$Q_{i,j}(t') = \frac{1}{T}\sum_{t=t'-\frac{T}{2}}^{t=t'+\frac{T}{2}} \{n_i(t) - \mu_i\}\left\{n_j(t) - \mu_j\right\} \quad (i, j = 1, 2, \cdots, N) \tag{5}$$

where μ_i is the temporal average of $n_i(t)$, N is the number of electrodes, T is the duration of sampled noise, and t' is the time at the center of the duration.

The signal covariance matrix, $\mathbf{R}$, is calculated using observed scalp potentials, the transfer function, and estimated noise covariance [18]. The covariance of the observed signals $\mathbf{P}$ is calculated by $\mathbf{P} = \mathrm{E}[\mathbf{g}\mathbf{g}^T]$. Substituting Eq. (1) into $\mathbf{P}$, we obtain

$$\mathbf{P} = \mathbf{A}\mathbf{R}\mathbf{A}^T + \mathbf{Q} \tag{6}$$

The signal covariance R can be obtained by

$$\mathbf{R} = \mathbf{A}^{-1}(\mathbf{P} - \mathbf{Q})(\mathbf{A}^{-1})^T \tag{7}$$

In the present study, we estimated the noise covariance using ICA as described in next section.

2.3 Independent Component Analysis

The PPF in Eq. (3) and the PWF in Eq. (4) require the noise covariance. However, the signal and noise components are intermingled in the observed EEG signals. In such cases, each component was separated by ICA, which extracts independent sources from the observed signal based on statistical independence of the original signal. FastICA algorithm was used for performing the estimation of ICA [24].

This algorithm is based on a fixed-point iteration scheme maximizing non-Gaussianity as a measure of statistical independence. Non-Gaussianity was measured using an approximation of negentropy. The outline of ICA algorithm is as follows: When independent sources **s** are mutually mixed by a mixing matrix **M**, the observed signal **g** is described by

$$\mathbf{g} = \mathbf{M}\mathbf{s} \tag{8}$$

First, the number of sources is decided using principal component analysis (PCA). In the PCA, the order of EEG signals is reduced to the number of independent components. The order was decided by the contribution ratio of the eigen values of the EEG. *Empirically*, when the contribution ratio of the eigen values is over 90%, the order is assumed to the number of signal sources. Moreover, the amplitude and the distribution of each separated component were evaluated based on the anatomical knowledge for order decision. The principal component **z** is expressed as

$$\mathbf{z} = \mathbf{V}\mathbf{g} \tag{9}$$

where **V** is the whitening matrix. Actually, **V** serves to reduce the dimensionality of the matrix. Next, independent signals are estimated using the appropriate restoring matrix **W**. Finally, the original signal is estimated as

$$\mathbf{s}_0 = \mathbf{W}\mathbf{z} \tag{10}$$

An inverse of the mixing matrix **M** is described by multiplying a whitening matrix **V** and a restoring matrix **W** ($\mathbf{M} = (\mathbf{W}\mathbf{V})^{-1}$). ICA was applied to EEG signals in order to extract the independent components (Fig. 1). These components were separated into the signal and the noise components according to a priori physiological information. Thus, we obtained the separated signal and noise components by applying a mixing matrix. To confirm the restorative ability, the noise covariance matrix was estimated from either the separated noise using ICA or the differential noise between the original EEG signal and separated signal as shown in Fig. 1. Moreover, the signal covariance in the PWF was calculated with either the measured EEG or the separated signal using ICA. Finally, the spatial inverse filter was designed using these signal and noise covariance matrices for high resolution cortical dipole imaging.

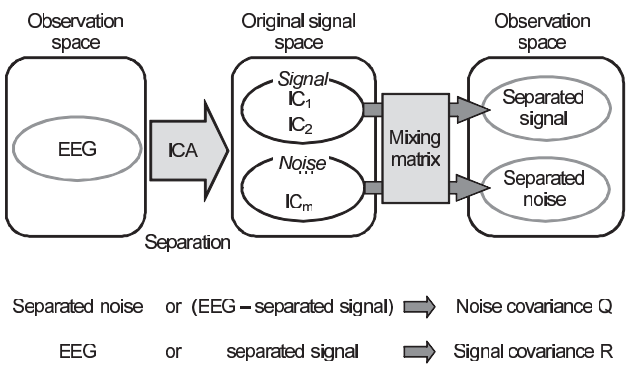

Fig. 1 Estimation of signal and noise covariance using ICA.

2.4 Simulation

In the inhomogeneous spherical source-conductor model, the radii of the brain, the skull, and the scalp spheres were taken as 0.87, 0.92, and 1.0, respectively [6], [11], [26]. The normalized conductivity of the scalp and the brain was taken as $\sigma_0 = 1.0$, and that of the skull as $\sigma_s = 0.0125$. The potentials on the scalp surface, generated by current dipoles inside the brain, can be calculated by solving the forward problem from the dipole source to the scalp-surface potential. 128 electrodes uniformly distributed over the upper hemisphere were used in the simulation. The scalp potentials were contaminated with Gaussian white noise (GWN). The noise level defined by $\|\mathbf{n}\|/\|\mathbf{g}\|$ was set to 0.05 to 0.2. A dipole layer with 1280 radial dipoles at a radius of 0.8 was used [12]. We compared the ability of spatial inverse filters under various signal and noise conditions. We evaluated the estimating abilities using the relative error between actual and estimated dipole layer distributions ($\|\mathbf{f} - \mathbf{f}_0\|/\|\mathbf{f}\|$) and maps of the estimated cortical dipole layer imaging.

In the primary simulation, two dipole sources were used to represent multiple localized brain electrical sources. The dipoles were oriented radially to the sphere. The eccentricity of both sources was set as 0.7 with the angle of $\pi/6$. The strength of each dipole was changed with sinusoid in time. The frequencies of fluctuation in the dipole moments were set to 13 Hz and 29 Hz that assuming EEG alpha and gamma activities, respectively. Data was corrected for 1 s with a sampling rate of 100 Hz.

Next, single dipole source was used to simulate the non-stationary time-varying signals. The dipole source was located at the elevation 20 degrees of posterior side with the eccentricity of 0.7. The dipole was oriented radially to the sphere. The strength of the dipole changed as the damped oscillation with the frequency of 13 Hz giving the evoked potentials or the event-related potentials. Data was collected for 0.4 s with a sampling rate of 1 kHz.

2.5 Human Experiments

Human visual evoked potential (VEP) experiments were carried out to examine the performance of the proposed restoration method. One healthy subject was studied in accordance with a protocol approved by the Institutional Review Board of the University of Illinois at Chicago. Visual stimuli were generated by the STIM system (Neuro Scan Labs, Inc.). 96-channel VEP signals referenced to right earlobe were amplified with a gain of 500 and band-pass filtered from 1 Hz to 200 Hz by Synamps (Neuro Scan Labs, Inc.), and were acquired at a sampling rate of 1 kHz by using SCAN 4.1 software (Neuro Scan Labs, Inc.). The electrode locations were measured using Polhemus Fastrack (Polhemus, Inc.) and best fitted on the spherical surface with unit radius. Half visual field pattern reversal check boards (black and white) with reversal interval of 0.5 sec served as visual stimuli and 400 reversals were recorded to obtain averaged

VEP signals. The display had a total viewing angle of 14.3 degree by 11.1 degree, and the check size was set to be 175' by 135' expressed in arc minutes. The EEG recordings were segmented into epochs of 0.4 s length including 0.1 s before and 0.3 s after stimuli onset.

3. Results

Primary, we compared the estimation results when the noise covariance of the PPF was calculated with the separated noise or the differential noise. Figure 2 shows the relative errors between the actual and estimated dipole distributions with respect to varying the noise level for GWN. Two radial dipole sources were used in this simulation. The order of ICA was estimated to be 4 from the contribution ratio of the eigen values in EEG. The relative error of the separated noise increased as the noise level became high. On the other hand, the relative error of the differential noise was stable whenever the noise level changed. The estimated dipole distributions in the case of the noise level of 0.1 are demonstrated in Fig. 3. The scalp potential was blurred and we cannot confirm two poles in Fig. 3 (a). When the noise covariance was estimated using separated noise the estimated result was very noisy as shown in Fig. 3 (c). Alternatively, when the noise covariance was estimated using the differential noise, the result in Fig. 3 (d) showed two localized areas and it was similar to the actual dipole distribution in Fig. 3 (b).

We compared the estimation results when the signal covariance of the PWF was calculated with EEG themselves or the separated signal. Figure 4 plots the relative errors with respect to varying the noise level for GWN. Figure 5 shows the estimated dipole distributions with the noise level of 0.1. When the signal covariance was estimated using the separated signal, the relative error and the dipole distribution demonstrated better performance than when using the EEG themselves.

Next, we examined the estimation results of the PWF with the signal in non-stationary conditions as shown in Fig. 6 (a). Figure 6 (a) shows 128-channel simulated EEG signals observed on the scalp surface. The order of ICA was estimated to be 2 from the contribution ratio of the eigen values in EEG. Figures 6 (b) and (c) show the separated signal components with ICA and the differential noise components between the measured EEG and the separated noise component, respectively. Figure 7 (a) shows simulation results of the relative error between the actual and estimated cortical maps against the center time of noise sample. The identification of the dipole imaging was carried out at 165 ms when first peak was observed in Fig. 6 (a). The noise level was

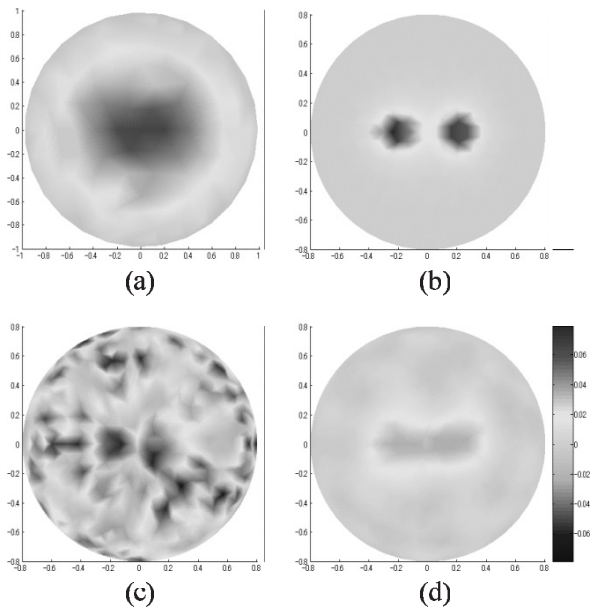

Fig. 3 Examples of the estimated inverse solutions of cortical dipole imaging using the PPF. (a) Scalp potential. (b) Actual dipole distribution. (c)–(d) Estimated dipole distribution. The noise covariance was calculated from (c) the separated noise and (d) the differential noise.

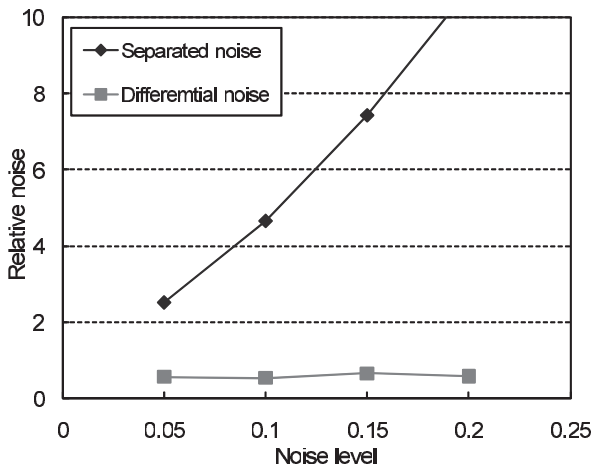

Fig. 2 Relative error between actual and estimated cortical maps using the PPF against the noise level. The noise covariance was calculated using the separated noise or the differential noise.

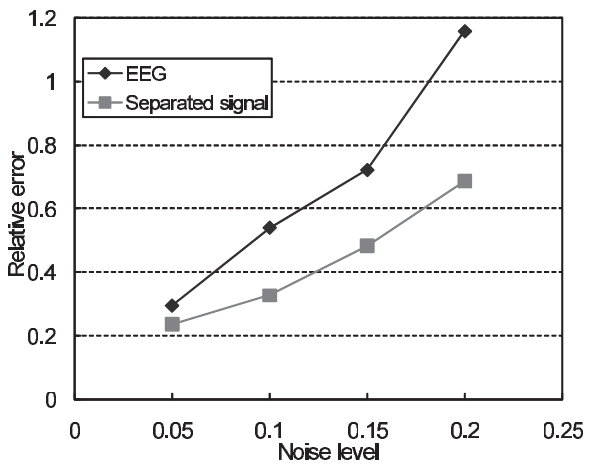

Fig. 4 Relative error between actual and estimated cortical maps using the PWF against the noise level. The signal covariance was calculated using the measured EEG or separated signal.

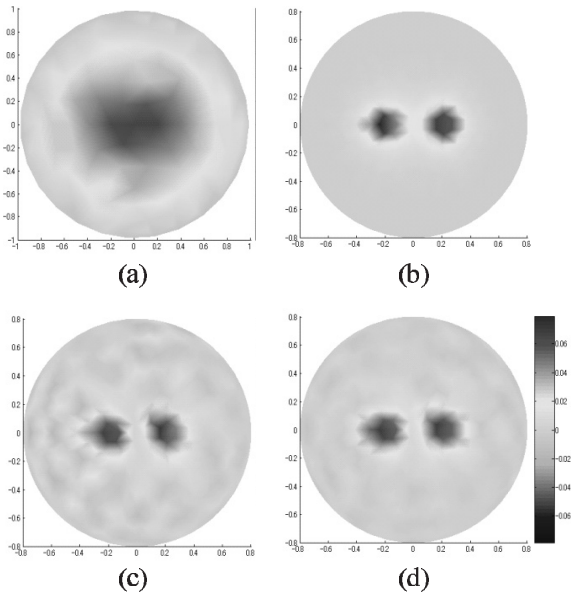

Fig. 5 Examples of the estimated inverse solutions of cortical dipole imaging using the PWF. (a) Scalp potential. (b) Actual dipole distribution. (c)–(d) Estimated dipole distribution. The signal covariance was calculated from (c) the measured EEG and (d) the separated signal.

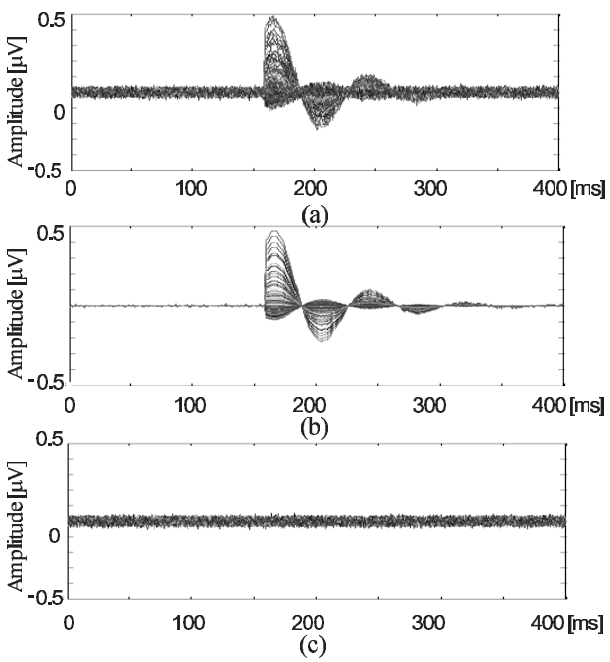

Fig. 6 Simulated EEG signals. (a) Simulated EEG signals contaminated with 10% GWN. (b) Separated signal components with ICA. (c) Differential noise components between (a) and (b).

0.1. The duration of noise sample was 80 ms. When the duration of noise sample included the imaging time instant of 165 ms, the relative errors were dramatically reduced to about 0.6. Figure 7 (b) plots the result when the identification of the dipole imaging was carried out at second peak (202 ms). In this case, the relative error was reduced around the imaging time of 202 ms. The duration of less error was

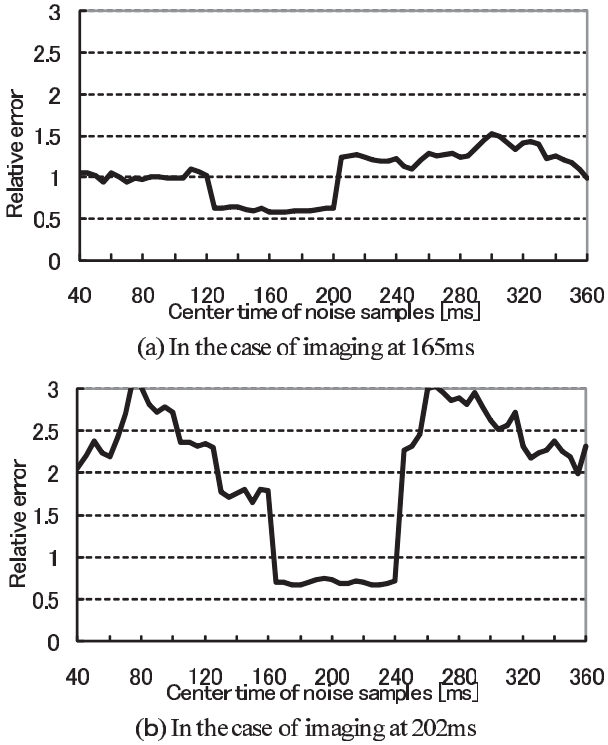

Fig. 7 Simulation results of relative error between actual and estimated cortical maps against the center time of noise sample. The dipole imaging was estimated at the time point around (a) 165 ms and (b) 202 ms. The duration of noise sample was 80 ms.

approximately 80 ms in both conditions. We confirmed the estimated cortical maps with the noise sample of the different time. Figure 8 (a) is the scalp potential and Fig. 8 (b) is the actual cortical dipole distribution. Figures 8 (c)–(e) show the cortical dipole distributions estimated using the noise covariance calculated with various noise sample. The maps were observed from the posterior side of 30 degrees in elevation. As shown in Fig. 8 (d), the estimated result using noise sample around 165 ms was the best for imaging at 165 ms data. We confirmed that the duration of noise sample should include the data at the imaging time even if source-free data are obtained at other time such as pre-stimulus data in evoked potentials. These results also imply that the dipole imaging have to hold at least the first peak of the evoked potential within the noise sample duration.

Figure 9 shows simulation results of the relative error between the actual and estimated cortical maps against the duration of noise sample. The dipole imaging was estimated at 165 ms. The noise was sampled including the imaging time. When the EEG signals were noisy in clinical measurements, the relative error could be reduced by the long duration of noise sample. Figure 10 shows dipole distributions at 165 ms estimated using the noise sample with various durations. The noise level was 0.1. When the duration of noise sample was set to 90 ms, the dipole distribution was localized and the noise was suppressed. The tendency of the accuracy of maps was similar to the plots of the relative error in Fig. 9. That is, the plot of the relative error

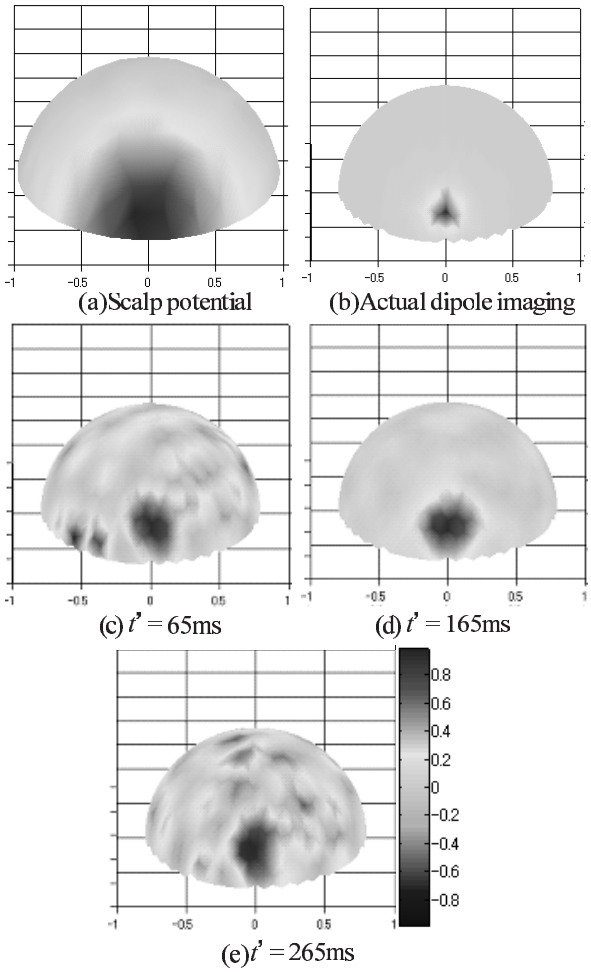

Fig. 8 Dipole distributions at 165 ms estimated with different time instants of noise sample. The duration of noise sample is T = 80 ms. (a) Scalp potential. (b) Actual dipole distribution. (c)–(e) Estimated dipole distribution using the PWF. The signal covariance was calculated using the noise around t' = (c) 65 ms, (d) 165 ms, and (e) 265 ms.

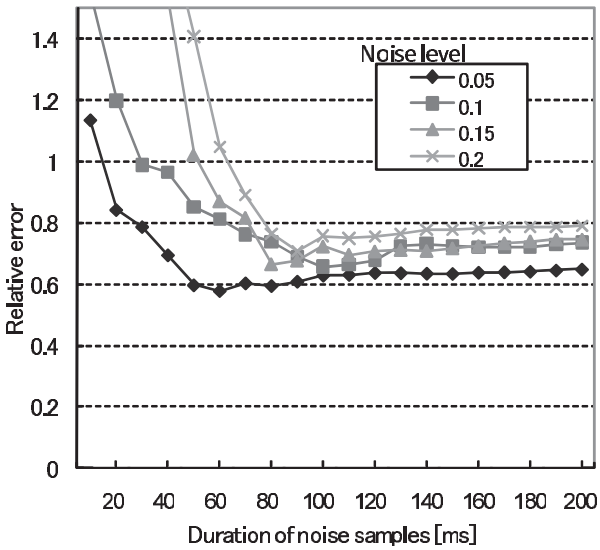

Fig. 9 Simulation results of relative error between actual and estimated cortical maps against the duration of noise sample. The dipole distribution was estimated at 165 ms. The noise level was set to 0.05, 0.1, 0.15, and 0.2. The noise was sampled including the imaging time.

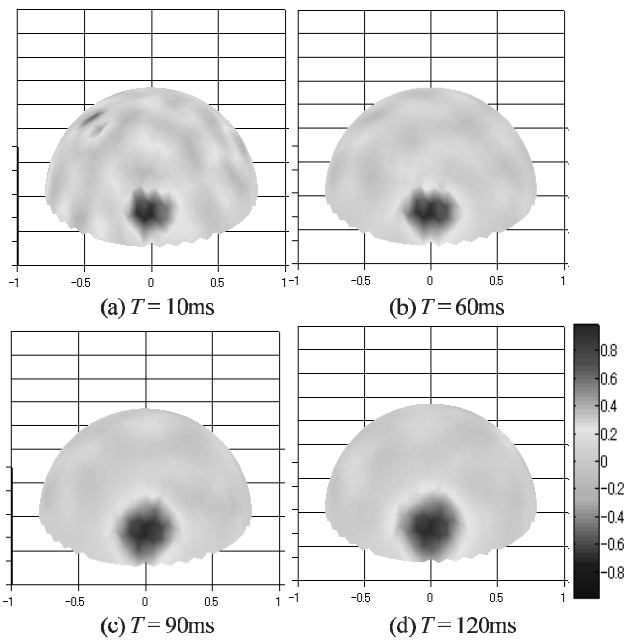

Fig. 10 Dipole distributions at 165 ms estimated using the noise sample with the duration T = (a) 10 ms, (b) 60 ms, (c) 90 ms, and (d) 120 ms. The time instant of noise sample is around 165 ms. The noise level was set to 0.1.

between the actual and estimated dipole distributions has a minimal value around 90 ms. These results indicated that the optimum sampling duration changed according to the noise level of the EEG signal.

By considering these simulation results, the cortical dipole imaging was applied to human experimental data. The order of ICA was estimated to be 3 from the contribution ratio of eigen values of the EEG. From the results of ICA, the amplitudes of first and second independent components were localized at the occipital lobe. On the other hand, third independent component had relatively small amplitude. Thus, we decided that first and second components were signal while third component was noise. Figure 11 shows examples of the estimated inverse solutions of cortical dipole distribution for visual evoked potential (VEP) at around 80 ms after visual stimuli, that is to say P100. The maps show the dipole distributions observed from the posterior side of 30 degrees in elevation. Figure 11 (a) shows the scalp potential of VEP. Figure 11 (b) shows the estimated dipole distribution using traditional method to evaluate the proposed method. In this method, **Q** was calculated from pre-stimulus data of the VEP. The estimation result using pre-stimulus data was noisy all over the brain surface and the distribution was not localized. Figure 11 (c)–(f) show estimated cortical dipole distribution using the PWF. **Q** was calculated with various duration of noise sample around the imaging time. As compared with the scalp potential in

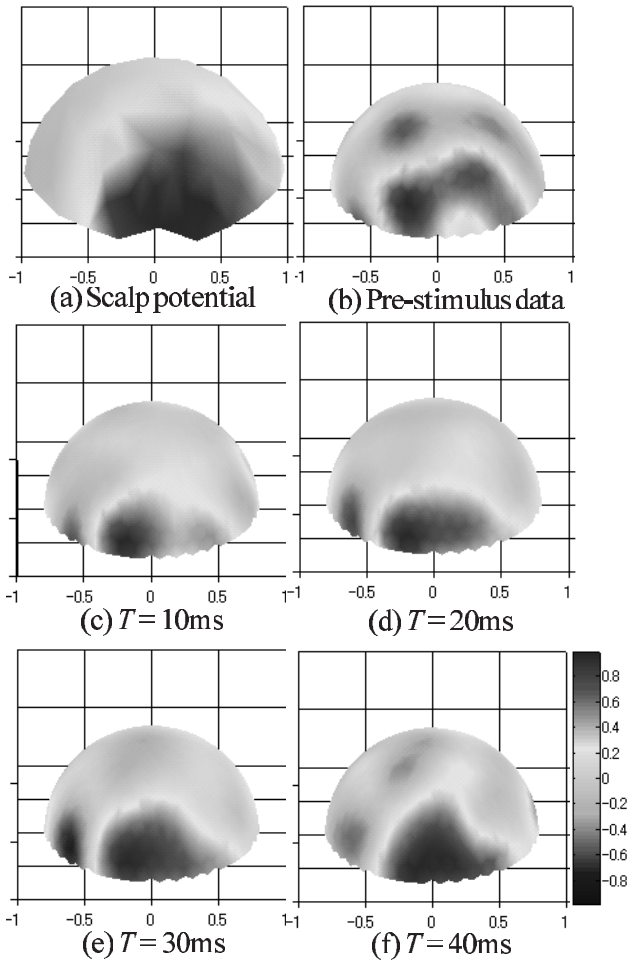

Fig. 11 Estimated inverse solutions of cortical dipole imaging for VEP. (a) Scalp potential. (b) Estimated dipole distribution with the **Q** calculated from pre-stimulus data. (c)–(f) Estimated dipole distribution using the PWF. **Q** was calculated using the differential noise with the duration T = (c) 10 ms, (d) 20 ms, (e) 30 ms, and (f) 40 ms.

Fig. 11 (a), the estimated dipole distribution performed well. Especially, when **Q** was calculated with the noise sample of 20 ms or 30 ms, the maps demonstrated the localized area around the visual field with less noise.

4. Discussion

We have investigated the cortical dipole imaging for high resolution visualization of the brain electrical activity. The cortical dipole distribution can represent dipole sources inside of the brain regardless of the number and the orientation of sources. In actual situation, cortical sources may have a strong tangential component. The brain electrical activity caused by the tangential dipole sources could also be represented with the strength distribution of radial dipoles [15]. When some dipole sources simultaneously exist in the brain, the distributions caused by each source may be overlapped on the scalp map. Moreover, in the case of the several dipole sources are synchronized, the distribution of original dipole sources may spread widely. In these cases, our proposed method can demonstrate the behavior of individual sources using equivalent dipole distribution. We confirmed that several dipole sources could be represented by the PPF-based inverse filters [15]–[17] and the PWF-based inverse filter [21].

We considered improving the precision of cortical dipole imaging by applying spatial inverse filters incorporated with statistical information of signal and noise. Both the PPF and the PWF require the statistical noise information described by the covariance **Q**. In a clinical situation, **Q** may be estimated from data that is known to be source free, such as pre-stimulus data in evoked potentials [28], [29]. However, if the EEG signals include the preparation potentials before stimuli such as event-related potentials or the EEG signals are in the steady state that continuously contained the signal components, it is difficult to extract the noise components. Moreover, it was difficult to segment the noise components from the EEG data because the spatiotemporal patterns of the signal and noise were overlapped. We examined new estimation methods based on ICA for the noise covariance matrix used in the PPF. Our estimation method provided the signal and noise components even if they are mixed with each other.

In order to extract the noise component for constructing the noise covariance matrix, it is necessary to remove most signal components. Therefore, the accuracy of signal separation using ICA exercises a great influence on the cortical dipole imaging. The order of ICA was determined from the contribution ratio of the eigen values. In simulations, the accuracy of separation can be evaluated by a relative error between the actual and estimated dipole distributions. The order of ICA should be higher than or equal to the number of signal sources. As a result of the experiments, the lower the order of ICA, the sharper the separated dipole distribution. It was the best when the number of the independent components was coincided with the number of the signal sources. However, the actual signal and noise components are unknown in clinical application and the number of the dipole sources may change depending on time. We checked the accuracy of signal and noise separation from the amplitude and the distribution of separated independent components referring to an anatomical knowledge.

The noise component was extracted from EEG signals using ICA. From the results of Figs. 2 and 3, it was better to use the differential noise between the EEG signal and the separated signal for calculating noise covariance in PPF rather than the separated noise. In the FastICA algorithm, PCA was used for reducing the dimension of the signals. Therefore, most of the noise components might be lost from the separating noise. Alternatively, since the differential noise included residual noise components, the noise covariance calculated with the differential noise was effective for the inverse estimation. In the PWF, the signal covariance is required in addition to the noise covariance. Fortunately, if the noise covariance was obtained, the signal covariance can be calculated using Eq. (7) proposed by Sekihara and Scholz [18]. In our simulation, the covariance of the ob-

served signals **P** was calculated with either the separated signal using ICA or the measured EEG as it is. When the cortical dipole distribution was estimated using the signal covariance based on the separated signals, the relative error was significantly reduced compared with that using the measured EEG as shown in Fig. 4. The noise of the dipole distribution was also suppressed while the spatial resolution was improved as shown in Fig. 5. It was confirmed that the results of the PWF in Fig. 5 (d) were better than that of the PPF in Fig. 3 (d). It was considered that the signal information was emphasized by applying the appropriate signal covariance to the PWF. The signal covariance may be directly estimated from the separated signal components using ICA. We need to examine the performance of this alternative estimation method in the near future.

We investigated the acquiring method of the noise data in order to calculate the noise covariance matrix **Q** built in the PPF and the PWF. The results shown in Fig. 7 indicates that the noise components for covariance estimation should be sampled to include the time point of the imaging because when the imaging was carried out at 165 ms and 202 ms the relative error was reduced around 165 ms and 202 ms, respectively. The duration of low relative error was coincides with the duration of the noise sample. The dipole map estimated with noise sample around the imaging time was obviously better than otherwise as shown in Fig. 8. Moreover, the result of Fig. 9 indicated that the duration of noise sample for covariance calculation had an optimum value and it was according to the noise level. That is, when the EEG signal was noisy, the duration of noise sample should be set to long. It was understood that the estimated maps were localized and noise-suppressed by adjusting the duration of noise sample according to the signal to noise ratio. In Fig. 10, cortical dipole maps were compared by changing the duration of noise sample for noise covariance calculation. When the duration was short, the signal was localized, but the noise was emphasized. Alternatively, when the duration was long, the signal was blurred, but the noise was suppressed. It was considered that the contribution of the noise suppression term $\gamma\mathbf{Q}$ in Eq. (4) increased by the long duration of noise sample. Moreover, the variation of noise was very sensitive for the short duration of noise sample. In conclusion, noise can be controlled at the sacrifice of localization of the signal by setting up the duration of noise sample for a long time.

In addition, the proposed method was applied to clinical data based on the above-mentioned results. In this case, the tendency of the experimental result by change of the duration of noise sample was the same as that of the computer simulation. When the duration of noise sample was set to $T = 40$ ms for calculating **Q**, the dipole distribution was blurred. Alternatively, when $T = 10$ ms or 20 ms, the peak of the dipole distribution was well-localized and they were better than the traditional method using the pre-stimulus data. The obtained result was in good agreement with a physiological knowledge. These results suggest that the noise components obtained from ICA can be used for noise covariance estimation.

Further investigations using a more realistic head conductor model and experimental data are necessary to validate the performance of the proposed model in cortical dipole source localization.

Acknowledgement

The authors would like to thank Prof. Bin He, University of Minnesota who provided the experimental data.

References

[1] P. Nunez, R.B. Silibertein, P.J. Cdush, R.S. Wijesinghe, A.F. Westdrop, and R. Srinivasan, "A theoretical and experimental study of high resolution EEG based on surface Laplacian and cortical imaging," Electroencephalogr. Clin. Neurophysiol., vol.90, pp.40–57, 1994.

[2] B. He, "Brain electric source imaging—Scalp Laplacian mapping and cortical imaging," Crit. Rev. Biomed. Eng., vol.27, pp.149–188, 1999.

[3] M. Hamalainen and R. Ilmoniemi, "Interpreting measured magnetic fields of the brain: Estimates of current distributions," Univ. Helsinki, Finland Tech. Rep. TKK-F-A559, 1984.

[4] R. Srebro, R.M. Oguz, K. Hughlett, and P.D. Purdy, "Estimating regional brain activity from evoked potential field on the scalp," IEEE Trans. Biomed. Eng., vol.40, no.6, pp.509–516, June 1993.

[5] A. Gevins, J. Le, N.K. Martin, P. Brickkett, J. Desmond, and B. Reutter, "High-resolution EEG: 124-channel recording, spatial deblurring and MRI integration method," Electroencephalogr. Clin. Neurophysiol., vol.90, pp.337–358, 1994.

[6] F. Babiloni, C. Babiloni, F. Carducci, L. Fattorini, C. Anello, P. Onorati, and A. Urbano, "High resolution EEG: A new model-dependent spatial deblurring method using a realistically-shaped MR-constructed subject's head model," Electroencephalogr. Clin. Neurophysiol., vol.102, pp.69–80, 1997.

[7] J.W. Philips, R.M. Leahy, J.C. Mosher, and B. Timsari, "Imaging neural electrical activity from MEG and EEG," IEEE Trans. Med. Imaging, vol.16, no.3, pp.338–348, 1997.

[8] G. Edlinger, P. Wach, and G. Pfurtscheller, "On the realization of an analytic high-resolution EEG," IEEE Trans. Biomed. Eng., vol.45, no.6, pp.736–745, June 1998.

[9] B. He, "High resolution imaging of brain electrical sources," IEEE Eng. Med. Biol. Mag., vol.17, no.5, pp.123–129, Sept./Oct. 1998.

[10] B. He, D. Yao, and J. Lian, "High resolution EEG: On the cortical equivalent dipole layer imaging," Clin. Neurophysiol., vol.113, pp.227–235, 2002.

[11] R. Sidman, M. Ford, G. Ramsey, and C. Schlichting, "Age-related features of the resting and P300 auditory evoked responses using the dipole localization method and cortical imaging technique," J. Neuroscience Methods, vol.33, pp.23–32, 1990.

[12] Y. Wang and B. He, "A computer simulation study of cortical imaging from scalp potentials," IEEE Trans. Biomed. Eng., vol.45, no.6, pp.724–735, June 1998.

[13] B. He, "Neural Engineering," Kluwer Academic Publishers, New York, NY, USA, 2005.

[14] J.Z. Wang, S.J. Willimnon, and L. Kaufman, "Magnetic source images determined by a lead-field analysis: The unique minimum-norm least-squares estimation," IEEE Trans. Biomed. Eng., vol.39, no.7, pp.665–675, July 1992.

[15] J. Hori and B. He, "Equivalent dipole source imaging of brain electric activity by means of parametric projection filter," Annals Biomed. Eng., vol.29, pp.434–445, 2001.

[16] J. Hori, M. Aiba, and B. He, "Spatio-temporal dipole source imaging of brain electrical activity by means of time-varying parametric pro-

jection filter," IEEE Trans. Biomed. Eng., vol.51, no.5, pp.768–777, May 2004.
[17] J. Hori and B. He, "EEG cortical potential imaging of brain electrical activity by means of parametric projection filters," IEICE Trans. Inf. & Syst., vol.E86-D, no.9, pp.1909–1920, Sept. 2003.
[18] K. Sekihara and B. Scholz, "Average-intensity reconstruction and Wiener reconstruction of bioelectric current distribution based on its estimated covariance matrix," IEEE Trans. Biomed. Eng., vol.42, no.2, pp.149–157, Feb. 1995.
[19] A.M. Dale and M. Sereno, "Improved localization of cortical activity by combining EEG and MEG with MRI cortical surface reconstruction: A linear approach," J. Cognitive Neuroscience, vol.5, pp.162–176, 1993.
[20] R. Grave de Peralta, R. Menendez, and S.L. Gonzalez Andino, "Distributed source models: Standard solutions and new developments," in Analysis of Neurophysiological Brain Functioning, ed. C. Uhl, pp.176–201, Springer, Berlin, 1998.
[21] J. Hori, T. Miwa, T. Ohshima, and B. He, "Cortical dipole imaging of movement-related potentials by means of parametric inverse filters incorporating with signal and noise covariance," Methods Inform. Med., vol.46, no.2, pp.242–246, 2007.
[22] B.D. Van Veen, W.V. Drongelen, M. Yuchtman, and A. Suzuki, "Localization of brain electrical activity via linearly constrained minimum variance spatial filtering," IEEE Trans. Biomed. Eng., vol.44, no.9, pp.867–880, Sept. 1997.
[23] K. Sekihara, D. Poeppel, A. Marantz, H. Koizumi, and Y. Miyashita, "Noise covariance incorporated MEG-MUSIC algorithm: A method for multiple-dipole estimation tolerant of the influence of background brain activity," IEEE Trans. Biomed. Eng., vol.44, no.9, pp.839–847, Sept. 1997.
[24] A. Hyvarinen, "Fast and robust fixed-point algorithms for independent component analysis," IEEE Trans. Neural Netw., vol.13, no.3, pp.626–634, 1997.
[25] M. Ungureanu, C. Bigan, R. Strungaru, and V. Lazarescu, "Independent component analysis applied in biomedical signal processing," Measurement Science Review, vol.4, sect. 2, pp.1–8, 2004.
[26] S. Rush and D.A. Driscoll, "EEG electrode sensitivity—An application of reciprocity," IEEE Trans. Biomed. Eng., vol.BME-16, no.1, pp.15–22, 1969.
[27] P.C. Hansen, "Truncated singular value decomposition solutions to discrete ill-posed problems with ill-determined numerical rank," SIAM J. Sci. Comput., vol.11, pp.503–518, Nov. 1990.
[28] A.N. Tikhonov and V.Y. Arsenin, Solutions of Ill-Posed Problems, Wiley, New York, 1977.
[29] E. Oja and H. Ogawa, "Parametric projection filter for image and signal restoration," IEEE Trans. Acoust. Speech Signal Process., vol.16, no.6, pp.338–348, 1997.

Junichi Hori received the B.E. and M.E. degrees in Information Engineering from Niigata University, Niigata, Japan, in 1986 and 1988, respectively. In 1996 he received the Ph.D. degree in Computer Science from the Tokyo Institute of Technology, Tokyo, Japan. In 1988 he joined the staff of the Department of Information Engineering, Niigata University, as a research associate. He is currently an associate Professor of Biocybernetics Department, Niigata University, Niigata, Japan. From 1999 to 2000, he was a Visiting Scholar in the Biomedical Functional Imaging and Computation Laboratory at the University of Illinois at Chicago. His research interests include inverse problem of physiological system, and biomedical signal processing, and neural engineering.

Kentarou Sunaga received the B.E. and M.E. degrees in engineering from Niigata University, Niigata, Japan, in 2006 and 2008, respectively. He is currently working for Hitachi Medical Corporation. His research interest includes human brain imaging.

Satoru Watanabe received the B.E. degree in engineering from Niigata University, Niigata, Japan, in 2009. He is currently working for Olympus Medical Systems Corporation. His research interest includes human brain imaging.